

MEA/SG CAPTURE CO₂ IN THERMAL ELECTROCHEMICAL CO-DRIVE SYSTEM

Wancheng Ding¹, Yunsong Yu^{1,*}, Zaoxiao Zhang^{1,2}, Geoff Wang³

1 School of Chemical Engineering and Technology, Xi'an Jiaotong University, No.28 Xianning West Road, Xi'an 710049, P.R. China

2 State Key Laboratory of Multiphase Flow in Power Engineering, Xi'an Jiaotong University, No.28 Xianning West Road, Xi'an 710049, P.R. China

3 School of Chemical Engineering, The University of Queensland, St Lucia, QLD 4072, Australia

(*)email: cloud.pine02@mail.xjtu.edu.cn

ABSTRACT

The Thermal Electrochemical Co-drive System (TECS) has the advantages of high desorption rate and low energy consumption. However, the fluid flow, heat and mass transfer performance is still unknown in TECS. Thus, a comprehensive experiment and simulation work on TECS is performed to demonstrate the fluid flow, heat and mass transfer performance in a pilot scale TECS. The reaction kinetics of the electrolyzed MEA/SG solution is discussed. A pilot-scale TECS is set up and gas-liquid two-phase flow model is developed for the TECS. According to the numerical computation and experiment, the gas-liquid two-phase flow field was analyzed under the thermal electrochemical co-drive conditions. The mechanism of heat and mass transfer was clearly understood. The synergy of thermal desorption and electrochemical desorption was quantified numerically. The results showed that the temperature of TECS was reduced below 60 °C and the energy consumption amount was determined at 1.3GJ/t to 2.1GJ/t, which is much lower than the conventional process. LNG cold energy reduced the desorption energy consumption.

Keywords: TECS, CO₂ capture, Numerical, Energy consumption

NONMENCLATURE

Abbreviations

| | |
|-------|--|
| PCC | Post combustion capture |
| A | Drive force for the CO ₂ desorption |
| a_1 | Effective area, m ² ·m ⁻³ |
| B | Source term, kg·Vm ⁻³ s ⁻¹ |

| | |
|-----------|---|
| B_r | Desorption source term, kg·Vm ⁻³ s ⁻¹ |
| C_M | Mass fraction of Monoethanolamine |
| C_S | Mass fraction of Sodium glycinate |
| C_A | Amine concentration, mol·L ⁻¹ |
| C_P | Specific heat capacity at constant pressure, J·kg ⁻¹ K ⁻¹ |
| D_1 | Diffusivity, m ² ·s ⁻¹ |
| D_{1r} | Desorption diffusivity, m ² ·s ⁻¹ |
| D_1 | Coefficient of diffusion, m ² ·s ⁻¹ |
| E | Electrical parameter |
| E_a | Activation energy, kJ·mol ⁻¹ |
| F | Force, kg·m ⁻² s ⁻² |
| F_e | Electrochemical force, kg·m ⁻² s ⁻² |
| H | Heat transfer source term, kW·m ⁻³ |
| h | Gas holdup |
| h_r | Gas holdup at desorption |
| I | Current, A |
| \bar{I} | Unit tensor, A |
| K | Kinetics |
| K_h | Heat transfer coefficient, K |
| P | Pressure, Pa |
| $q_1 q_2$ | Electric charge, C |
| R | Gas constant |
| R_0 | Correlation coefficient |
| k | Reaction rate constant |
| r | Reaction rate, mol·L ⁻¹ |

| | |
|----------|--|
| r_i | Distance, m |
| U | Velocity, $m \cdot s^{-1}$ |
| U_1 | Gas phase velocity, $m \cdot s^{-1}$ |
| U_g | Liquid phase velocity, $m \cdot s^{-1}$ |
| T | Temperature, K |
| T_e | Electrode temperature, K |
| T_f | Fluid temperature, K |
| n_0 | The amount of initial substance of SG, mol |
| n | SG consumption, mol |
| U_{lr} | Gas phase velocity at desorption, $m \cdot s^{-1}$ |
| U_{gr} | Liquid phase velocity at desorption, $m \cdot s^{-1}$ |
| Y | CO_2 concentration $mol \cdot L^{-1}$ |
| Y_e | CO_2 concentration at equilibrium state $mol \cdot L^{-1}$ |
| V | Electrode potential, mV |
| V_0 | Initial electrode potential, mV |
| V_r | Electrode potential at desorption state, mV |
| V_{or} | Initial electrode potential at desorption state, mV |
| α | Thermal diffusivity, $m^2 \cdot s^{-1}$ |
| Ω | Resistance |
| ω | Parameter |
| ρ | Density, $g \cdot cm^{-3}$ |
| ρ_r | Density at desorption, $g \cdot cm^{-3}$ |
| μ | Viscosity, $kg \cdot m^{-1} s^{-1}$ |

1. INTRODUCTION

Carbon dioxide (CO_2) is seriously produced during the burning of fossil fuels [1]. The most recognized methods for CO_2 capture include chemical absorption, physical and chemical adsorption, gas-separation membranes and mineralization. The most commonly applied technique is chemical absorption by solvents.

The general chemical absorption method is that the flue gas in the absorber contacts with amine solution counter currently to proceed the absorption reaction. After absorbing CO_2 , the rich liquid is sent to the stripper. In the stripper, the rich liquid contacts with the high-temperature steam counter-currently for desorption. The desorbed CO_2 is dehydrated and compressed to about 11MPa before being sent out for storage. The recycled lean liquid flows out from the

bottom of the stripper and is recycled and fed to the top of the absorber for recycling absorption.

Although chemical absorption is considered the most economical PCC technology, energy consumption and deployment costs are still too high [2,3]. The Thermal Electrochemical Co-drive System (TECS) [4] has the advantages of high desorption rate and low energy consumption by our previous theoretical analysis. In order to conduct an in-depth study of its electrochemical properties, a pilot-scale TECS was set up and a series of experiments and simulations were conducted. Since sodium glycinate (SG) solution has the advantages of low volatility and fast absorption rate [5], and the reaction enthalpy between SG and CO_2 is lower than that of MEA [6,7], the MEA/SG mixed solution is adopted in the experiment. Meanwhile, the CO_2 capture performance of MEA/SG solution was studied in the TECS. Finally, LNG cold energy is discussed for reducing the energy consumption.

2. EXPERIMENTAL

2.1 TECS system

A Thermal Electrochemical Co-drive System (TECS) experimental device was established in this work, The reactor is 60 cm high and 6 cm in diameter. As shown in the Fig. 1, the reactor consists of the main column, copper electrodes, graphite conductive sheets, and Pt100 temperature sensors. The jacket is arranged outside the column to heat the liquid. Several sets of copper electrodes are arranged inside the column. The arrangement of the copper electrodes not only reduces the backmixing, but also increases the turbulence of the electrolyte solution, and intensifies heat and mass transfer. A number of temperature sensors are installed in the column to record temperature changes. The entire column is made of visualized plexiglass materia. The CO_2 desorption process was recorded by the high speed camera.

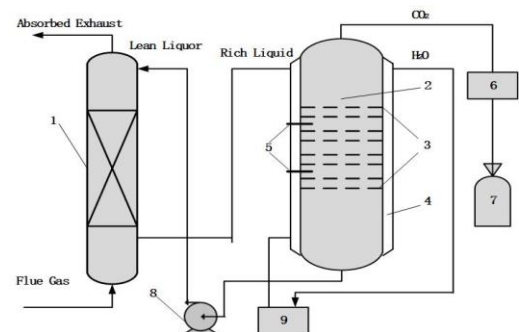


Fig. 1. Schematic of experimental setup of Thermal Electrochemical Co-drive System (TECS)

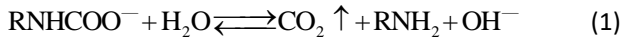
- 1.Absorber 2.Pumb 3.Copper electrode 4.Jacket
5.Temperature transducer 6.Catharometer 7. Gas tank
8.Reboiler 9.Water bath

2.2 Chemical reaction kinetics reaction experiment of SG

In order to investigate the desorption reaction kinetics of SG in the electrochemical condition, experiments were carried out. In the experiment, a certain amount of SG solution is prepared, and CO₂ is absorbed by the solution to be saturated. The graphite electrode is used at 335K-347K. When the electricity is supplied, a large amount of CO₂ bubbles are generated on the surface of the anode. The liquid phase mass spectrometry analysis is used to determine the components in the solution.

2.3 Reaction kinetics model

During the regeneration process, the reaction equation for releasing CO₂ is given as follows, in which CO₂ is mainly produced by the equation (1) [8].



Following the above reaction mechanism, the reaction kinetics equation can be written as

$$r = \frac{dc_A}{dt} = kc_A \quad (3)$$

According to the stoichiometry of reaction formula (1)

$$\frac{dn}{(n-n_0)} = -k dt \quad (4)$$

Then equation (5) can be obtained from the integration of equation (4)

$$\ln \frac{n}{n-n_0} = -kt \quad (5)$$

The experimental results are used to regress the reaction kinetics model above, which are given Table 1. The regression results are listed in Table 2.

Table 1 Experimental results of SG-CO₂ desorption in TECS

| No | Reaction conditions | CO ₂ /mol | n /mol | t /min | ln(n/(n-n ₀)) |
|----|-----------------------|----------------------|--------|--------|---------------------------|
| 1 | T=347.15K | 0.0327 | 0.0327 | 30 | 0.0325 |
| | P=1.0MPa | 0.0390 | 0.0390 | 50 | 0.0389 |
| | J=800Am ² | 0.0638 | 0.0638 | 70 | 0.0644 |
| 2 | T=341.15K | 0.0281 | 0.0281 | 30 | 0.0279 |
| | P=1.0MPa | 0.0384 | 0.0384 | 50 | 0.0382 |
| | J=800A/m ² | 0.0593 | 0.0593 | 70 | 0.0597 |
| 3 | T=335.15K | 0.0175 | 0.0175 | 30 | 0.0172 |
| | P=1.0MPa | 0.0268 | 0.0268 | 50 | 0.0265 |
| | J=800A/m ² | 0.0409 | 0.0409 | 70 | 0.0408 |

Table 2. The reaction rate constant k at different temperature

| T/K | Reaction kinetics equation | Correlation coefficient R ₀ | Kinetics constant k/min ⁻¹ |
|-----|--|--|---------------------------------------|
| 347 | $-\ln(1.023/(1.023-n))=(9.504t-23.4) \times 10^{-4}$ | 0.979 | 0.00095 |
| 341 | $-\ln(1.023/(1.023-n))=(7.949t+16.7) \times 10^{-4}$ | 0.989 | 0.00079 |
| 335 | $-\ln(1.023/(1.023-n))=(6.494t-40.6) \times 10^{-4}$ | 0.991 | 0.00064 |

It can be seen from Table 2 that the reaction kinetics equations of the SG rich solution follow the first-order reaction law at different reaction temperatures, and the R₀ is above 0.97, assuring the accuracy of the model.

The reaction rate of constants determined as

$$\ln k = -3.0707 \times 10^4 / RT + 3.6833 \quad (6)$$

where the reaction activation energy is determined as 30.707kJ/mol.

Finally, the reaction rate constant of the SG rich solution is correlated as:

$$k = 39.779 \exp(-3.0707 \times 10^4 / RT) \quad (7)$$

Based on the reaction kinetics model, the CO₂ desorption model in the reactor is developed to analyze the CO₂ desorption performance in TECS.

3. CO₂ DESORPTION MODEL

3.1 Gas and liquid two-phase flow model

The CO₂ desorption model is developed by considering the CO₂ concentration Y in the reactor, which is developed by including the electrochemical effects

$$\nabla \cdot \rho hUY = \nabla \cdot (\rho hD_1Y) + A \quad (8)$$

The A term above represents the drive force for the CO₂ desorption, which is developed by the reaction kinetics model in Section 2.2

$$A = Ka_1(Y - Y_c) \quad (10)$$

The continuity equation for the liquid phase is developed as

$$\nabla \cdot \rho hU = \omega A \quad (11)$$

The parameter ω is determined by the chemical reaction and molecular weight of the reactant and product.

Similarly, the electrical potential V in the reactor is also deduced by considering the effects between the two electrodes, which is

$$\nabla \cdot \rho hUV = \nabla \cdot (\rho hD_1V) + B \quad (12)$$

The term B presents the source term. it is developed by considering the fluid flow and electrochemical effects, which is developed as

$$B = (V - V_0)(\nabla U_l - \nabla U_g) \quad (13)$$

The energy equation of the liquid phase is developed as

$$\nabla \cdot \rho c_p h U T = \nabla \cdot \nabla (\rho c_p h \alpha T) + H \quad (14)$$

The heat transfer source term H is developed by the heat transfer occurring between the gas and liquid phases and the heat for the electrochemical drive force, which is given as

$$H = K_h S \Delta T + \frac{\delta I}{\Omega} dV \int dT (T_e - T_f) \quad (15)$$

The liquid flow is influenced by the interactive effects between two phases and electrochemical effects, which is expressed as

$$\begin{aligned} \nabla \cdot \rho h U U - \nabla \cdot h \mu \left(\nabla U + (\nabla U)^T - \frac{2}{3} \nabla \cdot U \bar{I} \right) \\ = -h \nabla P + F + F_e \end{aligned} \quad (16)$$

F refers to the body force, drag force and gravity. F_e represents the electrochemical force produced by the electrochemical effects for the liquid phase fluid flow, which is developed as

$$F_e = \frac{E q_1 q_2}{r^2} \quad (17)$$

where E is determined by the electrochemical potential. q_1 and q_2 refer to the charge of the ions influenced by the electrochemical effects.

As for the gas phase equations, only the source terms are revised by referencing the liquid phase equations above. For the gas phase continuity, the source term is the $-\omega A$. For the gas phase energy equation, the source term is the $-H$ due to the energy conservation. For the gas phase fluid flow equation, the source term is the $-F - F_e$.

The model includes the gas and liquid phase equations. According to the model, the effect of voltage, electrode distance and CO_2 loading are analyzed, which gives how to operate the CO_2 desorption effectively.

The numerical solution is performed for the gas and liquid two phases in the reactor. The finite volume method is used to discretize the differential equations. The SIMPLE algorithm is used to perform the numerical solution. The additional source term method is employed to improve the convergence. For the electrode set in the reactor, the no slip boundary condition is used. The grid independence analysis is done for the three sets of grid numbers as 120×25 , 100

$\times 20$ and 80×15 . It is found that the 100×20 is precision enough for the simulation. The mass imbalance is set at 1×10^{-5} , which is the convergence condition.

3.2 Model validation

In order to test the model, the experiment is performed at the positions of 5cm (a), 16cm (b), 29cm (c) and 42cm (d). The temperature is monitored by the thermal couples set along the reactor. The current, CO_2 loading and operating temperature are respectively varied from 130A/m^2 to 260A/m^2 , 0.3mol/mol to 0.5mol/mol 323K to 343K . The simulated temperature fits the experiment data very well at the points of a, b, c and d. The CO_2 desorption efficiency also fits the experiment data well, with maximum deviation of 5%. The results well validate the model, which proves its accuracy.

4. PERFORMANCE OF TECS

4.1 Temperature distribution

The temperature distribution is obtained in Fig. 2. As shown in Fig. 2, the temperature becomes low at the electrode zone. The temperature away from the electrode is higher than the zone around the electrode. This is due to the fact that the electrochemical effect for CO_2 desorption is strong around the electrode zone. It is found that the temperature difference is only about 5K, which is much lower than that at the conventional reactor. This result indicates that the energy dissipation due to the temperature difference is much lower in the electrochemical process, which is one of the reasons that the energy consumption is low.

4.2 CO_2 distribution

The CO_2 concentration is also simulated in the reactor. The results are provided in Fig. 3. As shown in Fig.3, the CO_2 concentration is higher in the zone around the electrode due to the strong electrochemical CO_2 desorption. For the upper and downer section of the electrode, the CO_2 concentration is higher in the downer section since the strong contact effects under the gas second flow. For the CO_2 concentration along the reactor height direction, the CO_2 concentration at the top of the reactor ranges from 0.85 to 0.92, which fits the experiment data and validates the high desorption efficiency. This is due to the strong electrochemical effects and the accumulation effects of the two phases.

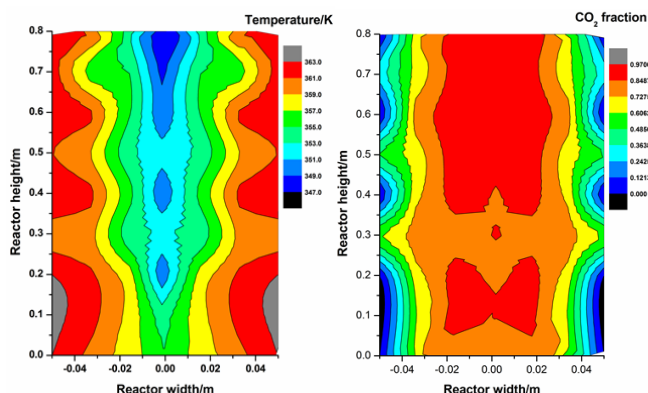


Fig. 2. Temperature distribution

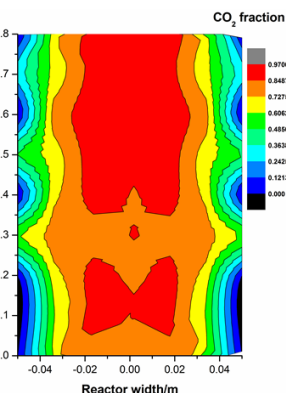


Fig. 3. CO₂ distribution

4.3 Fluid flow field

The gas and liquid velocity distribution is studied to demonstrate the gas and liquid two phases. The results are provided in Fig. 4 and Fig. 5. As shown in Fig. 4, the liquid velocity decreases from the top and decreases rapidly at the electrode section. However, the liquid accumulated at the electrode and then the liquid shows the higher flow velocity similar to the dispersion. Thus, the clear liquid velocity along the reactor height direction is determined and the low liquid velocity is identified at the electrode position.

For the gas velocity distribution, the electrode barricades the gas upper flow and makes the gas velocity produce second flow. Thus, the gas velocity shows the smaller velocity at the electrode position. The electrochemical effects around the electrode intensify the gas flow in the upper section of the electrode. This is due to the fact that the electrochemical effects produce the more CO₂ bubble and generate the pressure difference between the gas and liquid surface.

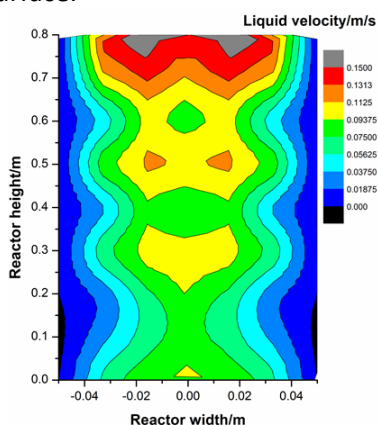


Fig. 4. Liquid velocity flow field

4.4 Electrical potential distribution

The electrical potential is also obtained by the simulation. The results are given in Fig. 6. As shown in

Fig. 6, the electrical potential is non uniform in the reactor. The electrical potential is higher at the zone near the electrode. This is the reason that the CO₂ desorption is very fast near the electrode. The electrochemical potential is highest at the bottom section and becomes smaller along the reactor height direction. The reason is that the ion concentrations and activities become smaller from the top to the bottom section of the reactor.

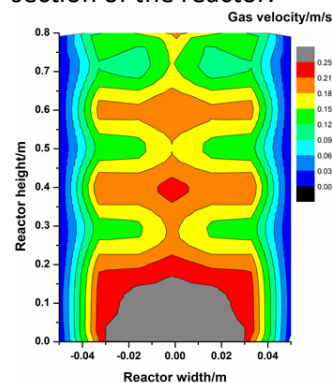


Fig. 5. Gas velocity flow field distribution

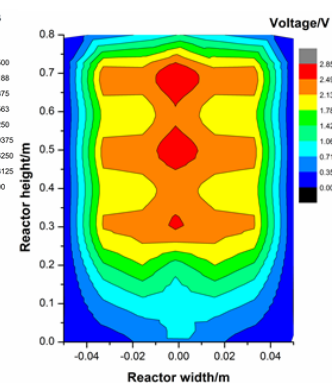


Fig. 6. Electrical potential

5. DISCUSSION

5.1 Energy consumption

The energy consumption is calculated by considering the consumption of electrical energy and heat. Considering the different CO₂ desorption temperature of 343K, 353K, 363K and 373K, the energy consumption is calculated and the result is provided in Table 3. As shown in Table 3, the energy consumption amount is determined at 1.3GJ/t to 2.1GJ/t, which is much lower than the conventional process in the literature [9,10].

Table 3. Energy consumption in electrochemical process for CO₂ capture

| Temperature /K | Energy consumption /GJ·t ⁻¹ | Source |
|----------------|--|-----------------------------------|
| 343 | 2.1 | This work |
| 353 | 2.0 | This work |
| 363 | 1.6 | This work |
| 373 | 1.3 | This work |
| 393 | 3.2 | Assessed by literature data[9,10] |

5.2 LNG cold energy utilization for CO₂ desorption

In the experiment, the SG and MEA rich liquid was found to reach the gel state at -40°C. Therefore, the

solution around the anode and cathode is physically separated. After that, the desorption operation was respectively performed for the rich liquid around the anode and the rich liquid around the cathode. The desorption amount of the CO₂ was measured. The experimental operation flow is provided in Figure 7.

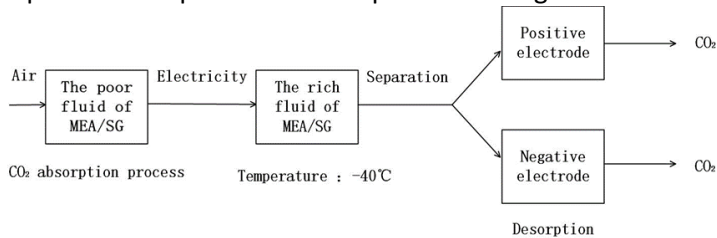


Fig. 7. The flow chart of MEA/SG solution desorption
The experimental results are given in Figure 8.

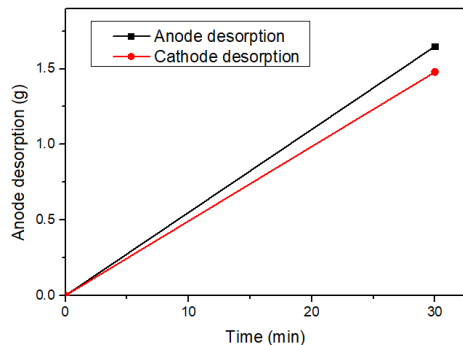


Fig. 8. The desorption capacity of the anode and cathode

According to the experimental results, it can be concluded that the total amount of CO₂ desorption of the rich liquid near the anode side is 11.48% higher than the total amount of the rich liquid near the cathode side. This is attributed to the fact that the concentration of RNHCOO⁻, HCO⁻³ and OH⁻ ions around the anode side is higher than that on the cathode side. Based on high desorption efficiency, the energy consumption of desorption can be reduced by using electrodes to separate the cations and anions.

In general, CO₂ is captured from the flue gases of power plant which means the flue gases are cooled by the LNG cold energy, hence the liquid CO₂ is obtained [11]. In the desorption process, we can also use the cold energy of LNG to enhance the desorption process.

This is quite economical since LNG cold energy is abundant, and proper utilization of LNG cold energy intensifies the desorption process without additional energy consumption [12].

6. CONCLUSIONS

Experiment, reaction kinetics model and developed gas-liquid two-phase flow model were used to understand the flow, heat transfer and mass transfer performance in TECS by MEA/SG. The temperature distribution, CO₂ concentration distribution, electrical

potential distribution and fluid flow field results in the tower were obtained. It was found that current density and CO₂ loading have great influence on CO₂ desorption. In TECS, the desorption temperatures reduced to below 363K. The energy consumption was obtained as 1.3GJ/t to 2.1GJ/t at 343K to 363K. The LNG cold energy is very effective to reduce the energy consumption in TECS.

ACKNOWLEDGEMENT

Financial support of the National Natural Science Foundation of China (No. 51506165) is gratefully acknowledged.

REFERENCE

- [1] Huancong Shi, Linna Zheng. Catalytic-CO₂-Desorption Studies of DEA and DEA-MEA Blended Solutions with the Aid of Lewis and Bronsted Acids. *Industrial & Engineering Chemistry Research*. 2018, 57(34):11505-11516
- [2] Yu YS, Li Y, Lu HF, et al. Performance improvement for chemical absorption of CO₂ by globalfield synergy optimization[J]. *International Journal of Greenhouse Gas Control*, 2011, 5 (4):649-658.
- [3] Yu YS, Li Y, Lu HF, et al. Multi-field synergy study of CO₂ capture process by chemical absorption[J]. *Chemical engineering science*, 2010, 65 (10): 3279-3292.
- [4] Liu GX, Yu YS. Thermal-Electrochemical Co-drive System for carbon capture[C]. 13th International Conference on Greenhouse Gas Control Technologies: Lausanne, 2016.
- [5] Majchrowicz, Magdalena E., Brillman, Wim. Amino Acid Salts for Carbon Dioxide Capture: Evaluating L-Proline at Desorber Conditions[J]. *Energy & Fuels*, 2015:3268-3275.
- [6] Ho-jun Song, Seungmoon Lee. Simplified Estimation of Regeneration Energy of 30 wt% Sodium Glycinate Solution for Carbon Dioxide Absorption. *Industrial and Engineering Chemistry Research*. 2008: 9925-9930
- [7] Zhang Xiaowen, Liu Helei. Reducing energy consumption of CO₂ desorption in CO₂-loaded aqueous amine solution using Al₂O₃/HZSM-5 bifunctional catalysts. *Applied Energy*, 2018:562-576
- [8] Zhao Wei, Shi Yao. Experimental Study on CO₂ Absorption and Regeneration of Aqueous Sodium Glycinate Solutions. *Journal of Chemical Engineering of Chinese Universities*, 2008 690-696
- [9] A. Baghban, S. Zilabi, S. Golrokhifar, S. Habibzadeh. Neural computations in modelling of CO₂ capture from Gas stream emissions by Sodium Glycinate solution. *Petroleum Science and Technology*. 36 (2018) 326-31.
- [10] M.S. Shaikh, A.M. Shariff, M.A. Bustam, G. Murshid. Physical Properties of Aqueous Blends of Sodium Glycinate (SG) and Piperazine (PZ) as a Solvent for CO₂ Capture. *Journal of Chemical & Engineering Data*. 58 (2013) 634-8.
- [11] Kanbur, B. B.; Xiang, L.; Dubey, S.; Choo, F. H.; Duan, F. Cold Utilization Systems of LNG: A Review. *Renewable Sustainable Energy Rev*. 2017, 79, 1171– 1188, DOI: 10.1016/j.rser.2017.05.161
- [12] Jinwoo Park, Inkyu Lee, Fengqi You. Economic Process Selection of Liquefied Natural Gas Regasification: Power Generation and Energy Storage Applications. *Ind. Eng. Chem. Res*. 2019, 58, 12, 4946-4956